ELSEVIER
SAUNDERS

Clin Chest Med 29 (2008) 181–193

CLINICS
IN CHEST
MEDICINE

Imaging of the Large Airways

Phillip M. Boiselle, MD

Department of Radiology, Beth Israel Deaconess Medical Center, Harvard Medical School, 330 Brookline Avenue, Boston, MA 02115, USA

Recent advances in multidetector-row CT technology and advances in post-processing techniques have revolutionized the ability to noninvasively image the large airways. This article provides a comprehensive review of imaging of the large airways. Introductory sections covering airway anatomy and CT imaging methods are followed by a review of tracheobronchial stenoses, neoplasms, tracheobronchomalacia, and congenital large airway abnormalities. Throughout, an emphasis is placed upon the complementary role of axial CT images and multiplanar reformation and three-dimensional reconstruction images for noninvasively assessing the large airways.

Anatomy

The trachea is a cartilaginous and fibromuscular tubular structure that extends from the inferior aspect of the cricoid cartilage to the level of the carina, a ridge that marks the origin of the main bronchi (Fig. 1) [1–3]. The trachea is comprised of 16 to 22 C-shaped cartilages, which are linked longitudinally by annular ligaments of fibrous and connective tissue [1–3]. The cartilages compose the anterior and lateral walls of the trachea and are connected posteriorly by the membranous wall of the trachea, which lacks cartilage and is supported by the trachealis muscle [1–3]. This muscle is composed of transverse smooth muscle fibers that narrow the tracheal lumen upon contraction [1–3]. The cartilaginous rings play a supportive function and help to maintain an adequate tracheal lumen during expiration. The posterior wall of the trachea either flattens or bows slightly forward during expiration in normal subjects (Fig. 2) [4,5]. During forced expiration, normal subjects have been shown to demonstrate a mean decrease in anteroposterior dimension of the tracheal lumen of about 35% [4]; however, in the setting of weakening or deficiency of the cartilaginous or membranous components of the airway, excessive expiratory collapsibility (>50% reduction), also referred to as tracheobronchomalacia, may be observed.

The trachea does not derive its blood supply from a single main vessel. Rather, it is supplied by a variety of vessels, including superiorly from the inferior thyroid arteries and right intercostal artery, and inferiorly from branches of the bronchial and intercostals arteries [2].

Normal tracheal measurements are reviewed in Box 1. The trachea is generally midline in position, but it is often displaced slightly to the right at the level of the aortic arch, with greater degree of displacement in the setting of a markedly tortuous, atherosclerotic aorta. The proximal trachea lies close to the skin surface, but the trachea angles posteriorly as it courses inferiorly in the thorax, eventually achieving a midcoronal location at the level of the carina (Fig. 3). Because of the angled course of the trachea, axial CT images do not provide a true perpendicular cross section of its lumen.

On axial CT images, the normal tracheal lumen usually demonstrates an oval, round (see Fig. 2a), or horseshoe shape [6]. The tracheal index can be calculated by dividing the coronal diameter (mm) by the sagittal diameter (mm). The normal value is approximately 1 [1,3–5]. A ''saber-sheath'' trachea (Fig. 4) refers to a configuration in which there is marked coronal narrowing and accentuation of the sagittal diameter (sagittal:coronal ratio >2) [10,11]. This finding is frequently associated with chronic obstructive

E-mail address: pboisell@bidmc.harvard.edu

0272-5231/08/$ - see front matter
doi:10.1016/j.ccm.2007.11.002

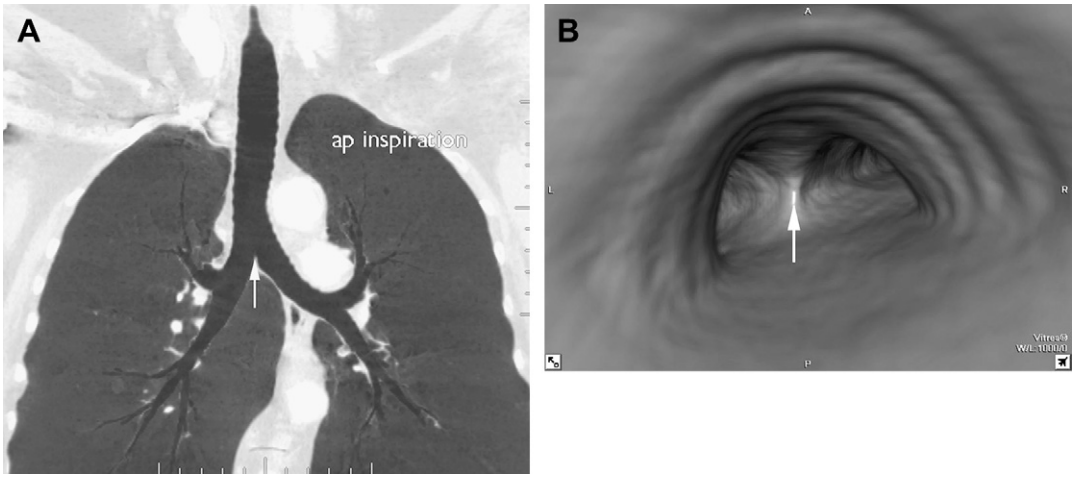

Fig. 1. Normal trachea. (*A*) Minimum intensity projection coronal oblique reformation CT image of the normal trachea and bronchi. Main bronchi originate from inferior trachea at level of carina (*arrow*). (*B*) Virtual bronchoscopic image shows internal perspective of lower trachea, carina (*arrow*), and proximal main bronchi.

lung disease. In contrast, a "lunate" trachea (Fig. 5a) refers to accentuation of the coronal diameter with a relative narrowing of the sagittal diameter (coronal:sagittal ratio >1) [12]. This finding is frequently associated with airway malacia (excessive expiratory collapsibility of the airway lumen) (see Fig. 5b).

The tracheal wall is composed of several layers, including an inner mucosa layer, followed by submucosa, cartilage or muscle, and an outer adventitia layer [13]. On axial CT images, the tracheal wall is usually visible as a 1- to 3-mm soft-tissue density stripe, demarcated internally by the air-filled tracheal lumen and externally by the adjacent fat-density of the mediastinum (Fig. 6) [13]. The posterior wall is typically thinner than the anterior and lateral walls. Cartilage within the tracheal wall may normally appear slightly denser than surrounding soft tissue and fat [13]. Calcification of cartilage may be observed in older patients, especially women [13].

Thickening of the airway wall (with or without calcification) is an important sign of tracheal pathology (Figs. 7 and 8). Importantly, axial images are the reference standard for assessing tracheal wall thickening, a finding that may be

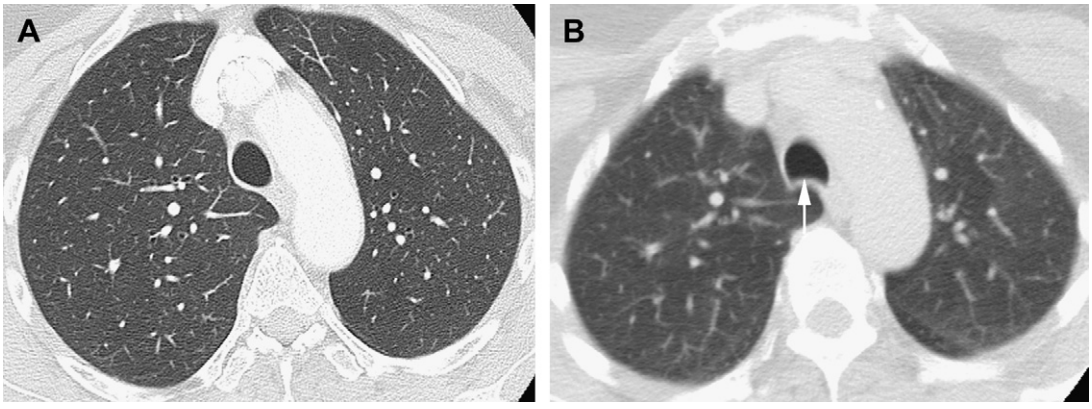

Fig. 2. Normal tracheal dynamics. (*A*) End-inspiratory image shows a round configuration of the tracheal lumen. (*B*) At end-expiration, the tracheal lumen has narrowed slightly, with anterior bowing of the posterior membranous wall (*arrow*).

Box 1. Normal tracheal measurements:

Length: 8–13 cm total
Extrathoracic 2–4 cm
Intrathoracic 6–9 cm

Diameter (average)
Men: 19.5 mm
13–25 mm coronal
13–27 mm sagittal
Women: 17.5 mm
10–21 mm coronal
10–23 mm sagittal

Data from Refs. [1,6–9].

overlooked at conventional bronchoscopy and three dimensional (3D) reconstruction images. The distribution of wall thickening can be helpful in limiting the differential diagnosis of the various causes of tracheal stenosis. For example, disorders of cartilage, such as relapsing polychondritis (see Fig. 7) and tracheobronchopathia osteochondroplastica (TBO), will spare the posterior membranous wall of the trachea, whereas other disorders generally result in circumferential thickening (see Fig. 8).

Fig. 3. Normal trachea. Minimum intensity projection sagittal oblique reformation CT image of the normal trachea (*arrow*) shows typical angled course of trachea from proximal anterior location to midcoronal position at level of carina.

Fig. 4. Saber sheath trachea. Axial CT image demonstrates elongated sagittal dimension of trachea with relative narrowing in the coronal plane, consistent with saber sheath configuration.

The main bronchi arise from the trachea at the level of the carina (see Fig. 1) and course obliquely to the axial plane. Because of the limitations of axial images for assessing structures that course obliquely, multiplanar and 3D reconstruction images are particularly helpful for evaluating caliber changes in the mainstem bronchi.

CT imaging methods

The recent advent of multidetector-row CT (MDCT) imaging has revolutionized noninvasive imaging of the central airways. With the latest generation of MDCT scanners, thin-section images of the entire central airways can be obtained in only a few seconds, creating an isotropic dataset in which the resolution is the same in the axial, coronal, and sagittal planes. Compared with standard helical CT scanners, MDCT provides higher spatial resolution, faster speed, greater anatomic coverage, and higher quality multiplanar reformation and 3D reconstruction images.

Axial CT images provide important anatomical information about the airway lumen, airway wall, and adjacent mediastinal and lung structures. Although axial CT images are still the reference standard for airway imaging, they have several important limitations, including limited ability to detect subtle airway stenoses, underestimation of the craniocaudad extent of disease, difficulty displaying complex 3D relationships of the airway, and inadequate representation of airways oriented obliquely to the axial plane

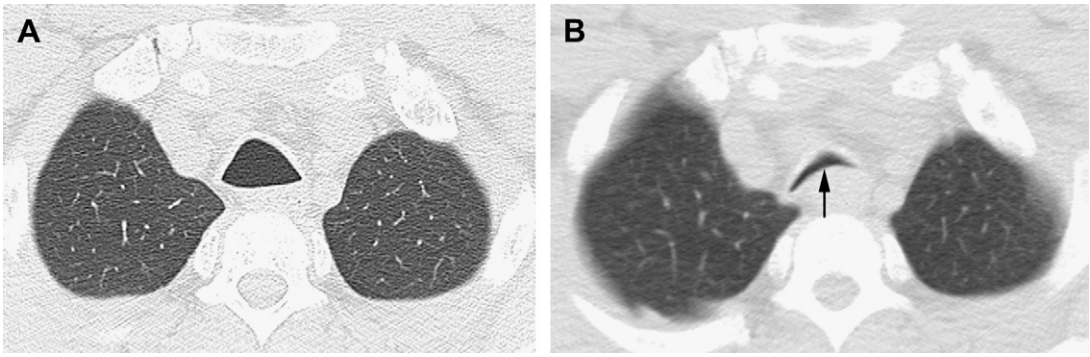

Fig. 5. Lunate trachea. (*A*) Axial end-inspiratory CT image shows elongated coronal dimension of trachea. (*B*) Axial dynamic expiratory CT image shows severe malacia, with excessive expiratory collapse of the tracheal lumen (*arrow*).

[14–22]. These limitations have important implications for assessing airway stenoses and complex, congenital airway abnormalities. Fortunately, multiplanar and 3D reconstruction images can overcome these limitations by providing a more anatomically meaningful display of the airways and adjacent structures [14–21]. These images have been shown to enhance the detection of airway stenoses, to aid the assessment of the craniocaudad extent of stenoses (Fig. 9), and to clarify complex, congenital airway abnormalities [19]. They have also been shown to improve diagnostic confidence of interpretation, enhance preprocedural planning for bronchoscopy and surgery, and improve communication among radiologists, clinicians, and patients [14–16].

Anatomical imaging of the airways is performed at end-inspiration; however, an additional expiratory imaging sequence should be performed for suspected airway malacia, which escapes detection on routine end-inspiratory sequences. As reviewed later in this article, dynamic expiratory imaging (imaging during a forced expiration) is superior to end-expiratory imaging (imaging after exhalation) for eliciting airway malacia [23–27].

Tracheobronchial stenosis

Tracheobronchial stenosis is defined as focal or diffuse narrowing of the tracheal lumen. It may occur secondary to a wide variety of benign and malignant causes (Box 2).

Axial CT images provide a precise anatomical display of the tracheal wall and lumen; however, as noted earlier in this article, they have a limited

Fig. 6. Normal trachea. Axial CT image shows normal thickness of tracheal wall. Note the "paper thin" quality of the posterior membranous wall (*black arrow*) and the slightly thicker anterior (*white arrow*) and lateral walls.

Fig. 7. Relapsing polychondritis. Axial CT image shows thickening of anterolateral tracheal walls with focal calcification (*arrow*). Note characteristic sparing of posterior membranous wall.

Fig. 8. Sarcoidosis. Axial CT image shows circumferential wall thickening of tracheal airway lumen.

ability to detect subtle airway stenoses, and frequently underestimate the craniocaudad extent of stenoses [14–20]. By providing a continuous anatomical display of the airways, multiplanar and 3D reconstruction images help to overcome these limitations [14]. In settings where such reconstructions are not possible, careful review of contiguous thin-section axial images can help to prevent the radiologist from overlooking stenoses.

CT evaluation of suspected tracheal stenosis is routinely performed at end-inspiration during a single breath hold. An additional sequence during dynamic expiration may be helpful to assess for tracheomalacia, which may coexist with tracheobronchial stenoses, especially among patients who have relapsing polychondritis, post-intubation stenosis, and airway narrowing secondary to long-standing extrinsic compression

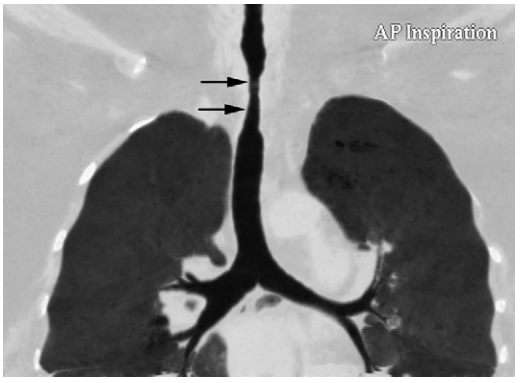

Fig. 9. Subglottic stenosis caused by prior tracheostomy tube. Minimum intensity projection, coronal reformation image of trachea shows moderate tracheal stenosis (*arrows*). Severity and craniocaudad length of stenosis were underestimated on axial CT images (not shown).

Box 2. Causes of tracheobronchial stenosis:

Iatrogenic
- Post-intubation[a]
- Lung transplantation

Idiopathic

Infection
- Laryngotracheal papillomatosis[b]
- Rhinoscleroma
- Tuberculosis

Neoplasm
- Primary tracheal neoplasm (squamous carcinoma, adenoid cystic carcinoma)
- Direct invasion (lung, esophagus, thyroid)
- Secondary neoplasm (breast, renal, melanoma, thyroid)

Saber sheath deformity

Systemic diseases
- Amyloidosis
- Inflammatory bowel disease
- Relapsing polychondritis
- Sarcoidosis
- Wegener granulomatosis

Tracheobronchopathia osteochondroplastica

Trauma

[a] Most common etiology.
[b] Although papillomas represent growth of new tissue, laryngotracheal papillomatosis is most frequently categorized as a non-neoplastic disease.

(eg, thyroid enlargement or mediastinal aortic vascular anomalies) [28,29].

It is important to accurately assess the location, length, and distribution of the stenosis, as well as the presence, distribution, and type of wall thickening. A consideration of these factors, in combination with ancillary thoracic findings and pertinent clinical and laboratory data, will allow the radiologist to effectively narrow the broad differential diagnosis of tracheobronchial stenosis to a few likely entities. In certain cases, such as relapsing polychondritis or TBO, a confident diagnosis can be made on the basis of imaging findings alone.

Although there is significant overlap in the imaging features of many causes of tracheobronchial stenosis, several key imaging features can help to effectively narrow this broad differential diagnosis. These features include: sparing of the posterior membranous wall (typical of relapsing polychondritis and TBO) (see Fig. 7), "hourglass" configuration (post-intubation stenosis), and calcification (relapsing polychondritis, TBO, amyloid, and tuberculosis). Additionally, systemic disorders (eg, amyloid, inflammatory bowel disease, polychondritis, sarcoid [see Fig. 8], tuberculosis, Wegener granulomatosis) are often associated with characteristic ancillary imaging and laboratory findings that may suggest their diagnosis.

Post-intubation stenosis is by far the most common cause of acquired tracheal stenosis, and may occur following endotracheal intubation or tracheostomy tube placement (see Fig. 9) [30]. It typically occurs secondary to injury of the trachea from the high pressure of an endotracheal tube balloon against the wall of the trachea [30,31]. This initially results in mucosal necrosis, followed by scarring and stenosis [30,31].

A recent study comparing MDCT with the gold standard of bronchoscopy showed a high sensitivity (92%) and specificity (100%) for detection of post-intubation stenosis [32]. The most common CT finding in post-intubation stenosis is a focal area of proximal tracheal luminal narrowing measuring approximately 2 cm in craniocaudad length [13,30,31]. The focal nature and circumferential narrowing typically produces a characteristic hourglass configuration. Less common findings include a thin membrane projecting into the tracheal lumen or a long segment of eccentric soft-tissue thickening [30,31].

Tracheobronchial neoplasms

Tracheobronchial neoplasms are rare. For example, it has been estimated that a primary tracheal tumor is roughly 180 times less common than a primary lung cancer [33]. A neoplasm within the central airways is more likely caused by direct airway invasion by an adjacent secondary neoplasm originating from the thyroid, lung, or esophagus [34].

A majority of primary tracheal neoplasms in adults are malignant, whereas the opposite is true in children [30,35]. Although a wide variety of neoplasms may arise in the central airways, five histologies compose the majority of primary tracheobronchial neoplasms: squamous cell carcinoma, adenoid cystic carcinoma, carcinoid, mucoepidermoid carcinoma, and squamous cell papilloma [36]. The most common cell type is squamous cell carcinoma, which is associated with cigarette smoking [30,35]. The second most common cell type is adenoid cystic carcinoma (Fig. 10), which is not associated with smoking [30,35]. It has a better prognosis than squamous cell carcinoma, but late recurrence is relatively common. The most common benign tracheal neoplasm is squamous cell papilloma, which is associated with cigarette smoking [30,35]. Carcinoid tumors are neuroendocrine neoplasms that most commonly arise within the main and lobar bronchi (Fig. 11), but about 15% develop within the segmental bronchi or lung periphery [37,38]. They are not associated with cigarette smoking.

MDCT is the imaging modality of choice for detection and staging of central airway neoplasms. Multiplanar reformation and 3D reconstruction images complement conventional axial images by providing a more anatomically meaningful display of the neoplasm and its relationship to adjacent structures, and by accurately determining the craniocaudad extent of disease [14]. Virtual bronchoscopy images provide a unique intraluminal perspective of the tumor. These images also play a potentially complementary role to conventional bronchoscopy by providing assessment of distal airways beyond a high-grade luminal narrowing or obstruction. Moreover, this method can provide a more global perspective of an endoluminal lesion than conventional bronchoscopy.

Surgery is the optimal therapy for both benign and malignant airway neoplasms [35,39,40].

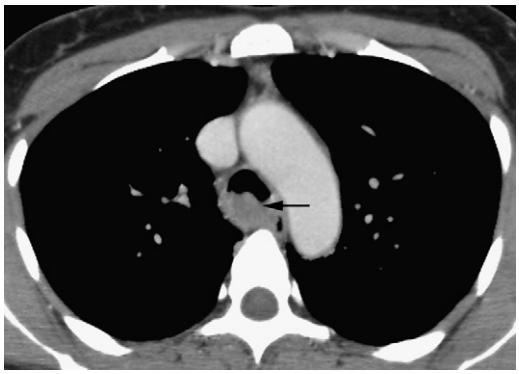

Fig. 10. Adenoid cystic carcinoma. Axial CT at level of aortic arch shows a lobulated, intraluminal mass (*black arrow*).

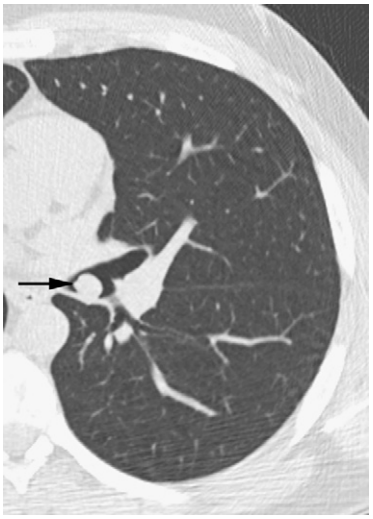

Fig. 11. Carcinoid tumor. Axial CT demonstrates a round, smoothly marginated, intraluminal lesion (*arrow*) in distal left main bronchus.

Radiation therapy may be administered to patients who have unresectable disease or as an adjunct to surgery, particularly in patients who have adenoid cystic carcinoma [39].

MDCT can determine whether a tumor is amenable to complete surgical resection, as well as the approach, type, and extent of surgical resection. MDCT provides critical information for the surgeon, including precise delineation of the 3D size of the neoplasm, including the craniocaudal length, and its relationship with other vital structures, including vascular structures. MDCT accurately defines the intraluminal and extraluminal extension of tumor, as well as post-obstructive complications such as atelectasis, pneumonia, and mucous plugging. Although MDCT can reliably detect the presence of lymphadenopathy, it cannot distinguish between hyperplastic and malignant nodes. Hyperplastic nodes are frequently seen in the setting of postobstructive pneumonitis from an endoluminal neoplasm. Additionally, MDCT does not reliably detect microscopic mediastinal invasion or neural invasion [41]. MDCT may detect pulmonary and extrapulmonary metastases, thereby enhancing tumor staging.

When a discrete tracheal mass is identified on imaging studies, the diagnosis of a primary tracheal neoplasm can usually be made with a high degree of confidence. CT can frequently suggest whether a tracheal lesion is malignant or benign [39]. Although some overlap exists, benign lesions are typically less than 2 cm in diameter, with well-defined, smooth borders, and without evidence of contiguous tracheal thickening or mediastinal invasion. In contrast, malignant lesions usually vary in size between 2 and 4 cm in diameter, with a flat or polypoid shape and irregular or lobulated borders (see Fig. 10). Contiguous tracheal wall thickening and mediastinal invasion are frequently observed. Although CT usually cannot distinguish between neoplastic cell types, detection of fat within a lesion on CT is nearly pathognomonic for a hamartoma or lipoma, and identification of calcification within a lesion is highly suggestive of a chondroid tumor (chondroma, chondrosarcoma). Vigorous enhancement of a bronchial neoplasm is typical of a carcinoid tumor.

In a minority of cases, tracheal neoplasms present as eccentric or circumferential tracheal wall thickening rather than a discrete mass. In such cases, the differential diagnosis includes tracheal stenosis from a variety of nonmalignant entities. In general, the presence of marked irregularity of tracheal wall thickening and the presence of extratracheal extension favor a primary tracheal neoplasm, but biopsy is usually necessary to establish the diagnosis.

Tracheobronchomalacia

Trachebronchomalacia refers to weakness of the airway walls or supporting cartilage, and is characterized by excessive expiratory collapse (see Figs. 5; Figs. 12 and 13) [28,29,42,43]. It may be either congenital or acquired. The acquired form is associated with a variety of risk factors and comorbidities, most notably chronic obstructive pulmonary disease (Box 3) [28,29,42]. Because it cannot be detected with routine end-inspiratory imaging studies, tracheobronchomalacia is widely considered an underdiagnosed condition [42,44–47].

Although bronchoscopy with functional maneuvers can reliably detect tracheobronchomalacia, it is not clinically feasible or desirable to perform this invasive test in all patients who present with chronic cough and other nonspecific respiratory symptoms. Recently, MDCT has been shown to noninvasively diagnose tracheobronchomalacia with similar sensitivity to conventional bronchoscopy [48–50].

Changes in size of malacic trachea and bronchi depend on the difference between the intraluminal

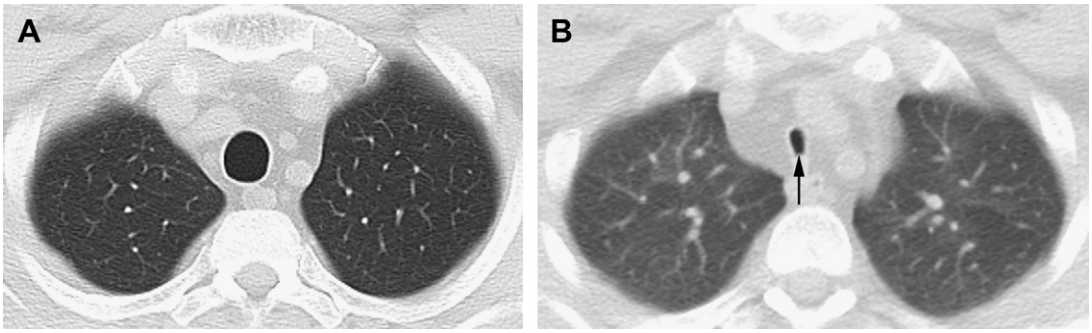

Fig. 12. Tracheomalacia. (*A*) End-inspiratory image of proximal trachea is normal. (*B*) Dynamic expiratory image shows excessive expiratory collapse with circumferential narrowing of trachea lumen (*arrow*).

pressure inside the airways and the pleural (intrathoracic) pressure outside [23,28]. Pleural pressure depends mostly on respiratory muscles, and is high during expiratory efforts. In contrast, intraluminal pressures are highly variable, and depend on airflow. When airflow is zero, intraluminal pressure equals alveolar pressure, and differs from pleural pressure only by the elastic recoil pressure of the lung, which depends on lung volume. At maximal lung volume with no flow (end-inspiration), the intraluminal pressure is 20 to 30 cm H_2O greater than pleural pressure, and the pressure difference expands the trachea. At low lung volumes with no flow (end-expiration), the intraluminal pressure is nearly equal to pleural pressure, and the trachea is unstressed. The trachea is most compressed during cough and dynamic expiration at low lung volume, when pleural pressure is high ($\sim$100 cm H_2O), and expiratory flow limitation in the small airways prevents transmission of the high alveolar pressures to the central airways. Under these conditions, intraluminal pressure is nearly atmospheric, and the large transmural pressure causes tracheal collapse [51].

Baroni and colleagues [23] directly compared the ability of end-expiratory and dynamic expiratory CT imaging methods to elicit tracheobronchomalacia. Consistent with the principles of respiratory physiology, their study showed that dynamic expiratory CT elicited a significantly greater degree of tracheal collapse than end-expiratory CT.

The vast majority of studies reported in the literature support the use of a threshold of greater

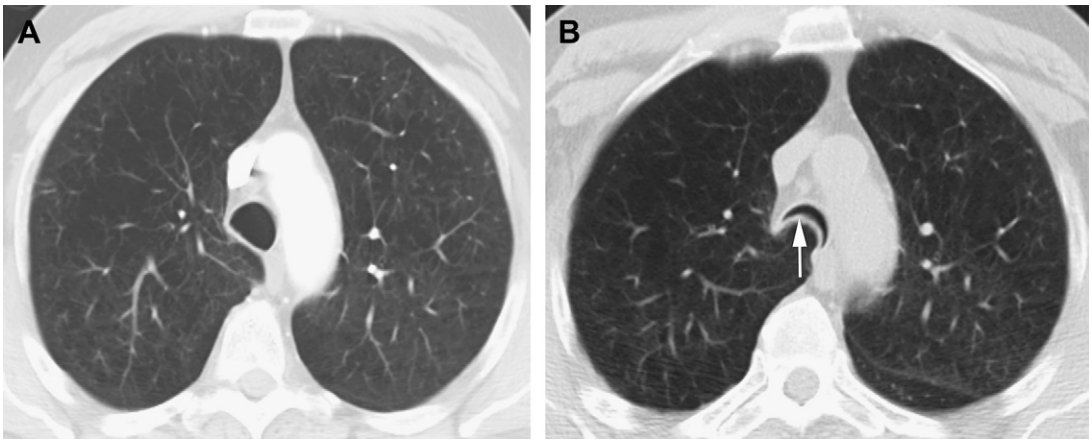

Fig. 13. Frown sign. (*A*) End-inspiratory image of the trachea is normal. Note the presence of emphysema. (*B*) Dynamic expiratory CT image demonstrates frownlike configuration of proximal trachea caused by excessive anterior displacement of posterior membranous wall that parallels the convex contour of the anterior wall, resulting in a characteristic crescentic lucency (*arrow*) that mimics a frown.

Box 3. Risk factors for acquired tracheomalacia

Chronic obstructive lung disease
Post-traumatic and latrogenic
Post-intubation
Post-tracheostomy
Radiation therapy
External chest trauma
Post-lung transplantation

Chronic infection/bronchitis
Chronic inflammation
Relapsing polychondritis

Chronic external compression of the trachea
Paratracheal neoplasms (benign and malignant)
Paratracheal masses (eg, goiter, congenital cyst)
Aortic aneurysms and vascular rings
Skeletal abnormalities (eg, pectus, scoliosis)

than or equal to 50% collapse as diagnostic of tracheobronchomalacia when using either bronchoscopy or CT; however, several studies have advocated the adoption of different threshold values, and there are only limited data in the literature regarding the normal range of dynamic expiratory collapse [2,52,53]. Based on available data in the literature, it is reasonable to employ a diagnostic threshold of greater than 50% expiratory luminal collapse, keeping in mind that some normal individuals may exceed this threshold.

Interpretation of CT images for the diagnosis of tracheobronchomalacia requires careful review and comparison of both end-inspiratory and dynamic expiratory images. The tracheal lumen is almost always normal in appearance on end-inspiration CT in patients who have tracheobronchomalacia (see Figs. 12a and 13a) [54]. Notable exceptions include: patients who have relapsing polychondritis who may demonstrate characteristic wall thickening and calcification that spares the posterior membranous wall of the trachea; patients who have lunate tracheal shape (coronal > sagittal dimension), which is frequently associated with tracheomalacia (see Fig. 5); and patients who have extrinsic tracheal compression from adjacent vascular anomalies or thyroid masses, in whom long-standing compression has been complicated by tracheomalacia.

The most accurate means for diagnosing malacia on CT is to use an electronic tracing tool to calculate the cross-sectional area of the airway lumen on images at the same anatomic level obtained at inspiration and dynamic expiration [29]. Such tools can be found on commercially available picture archival computer system (PACS) stations and dedicated post-processing workstations. Care should be taken to ensure that the same anatomical level is compared between the two sequences by comparing vascular structures and other anatomical landmarks.

In the setting of severe malacia, in which there is near complete collapse of the airway lumen during expiration, the diagnosis can be confidently made based on visual analysis of the images. It has recently been shown that about half of patients who have acquired tracheomalacia will demonstrate a characteristic expiratory "frownlike" configuration, in which the posterior membranous wall is excessively bowed forward and parallels the convex contour of the anterior wall with less than 6 mm distance between the anterior and posterior walls (see Fig. 13) [54]. This appearance, which has been termed the "frown sign," is highly suggestive of tracheomalacia, and can suggest the diagnosis of tracheomalacia on routine CT scans if patients inadvertently exhale [54]. Ideally, however, the diagnosis of tracheomalacia should be confirmed and quantified by a dedicated CT tracheal study.

When interpreting CT scans of patients who have tracheomalacia, it is important to report the severity, distribution, and morphology. These factors have an important impact upon treatment decisions, which are based upon a combination of symptoms, severity and distribution of disease, and underlying cause of tracheomalacia [55]. Patients who have severely symptomatic diffuse tracheomalacia characterized by excessive mobility and weakening of the posterior membranous wall may benefit from tracheoplasty, a surgical procedure that reinforces the posterior wall of the trachea with Marlex graft [56].

Congenital anomalies

A variety of congenital anomalies may affect the central airways, including branching anomalies, congenital stenosis, congenital malacia, congenital tracheobronchomegaly, and congenital diverticula.

Tracheal bronchus

Tracheal bronchus refers to an anomalous bronchial origin from the trachea, carina, or main bronchi. The anomalous origin is usually located within 2 cm of the carina [11,57–59]. Most commonly, this occurs as a displaced bronchus arising from the lower trachea and supplying the right upper lobe apical segment. Less commonly, the entire right upper lobe bronchus may be displaced, a configuration that is also referred to as a "pig bronchus" (Fig. 14). Although usually an asymptomatic and incidentally detected finding, impaired drainage may result in recurrent infections in some cases. Additionally, following endotracheal intubation, atelectasis may occur in the portion of lung supplied by the aberrant bronchus because of inadvertent obstruction by the balloon cuff.

Congenital tracheal stenosis

Congenital tracheal stenosis is a rare disorder that is characterized by complete tracheal rings associated with absent or deficient tracheal membranes [60–62]. It ranges in length from short to long segment stenosis. It typically presents during the first year of life and is associated with a high mortality rate. Symptoms include stridor, wheezing, cyanosis, and recurrent pneumonia. Adult presentation is rare, but is more common with short segment stenosis (Fig. 15) [62].

CT is highly sensitive for evaluating the length and extent of narrowing, as well as for identifying associated cardiopulmonary anomalies, including pulmonary artery sling. On axial CT images, there is narrowing of the tracheal lumen with an O-shaped configuration and absence of airway wall thickening. Virtual bronchoscopy is diagnostic by showing concentric rings extending along the posterior wall of the trachea. Surgical treatment usually involves resection of the involved segment or a slide tracheoplasty [62]. Asymptomatic pediatric patients may be followed by CT to noninvasively monitor tracheal growth [63].

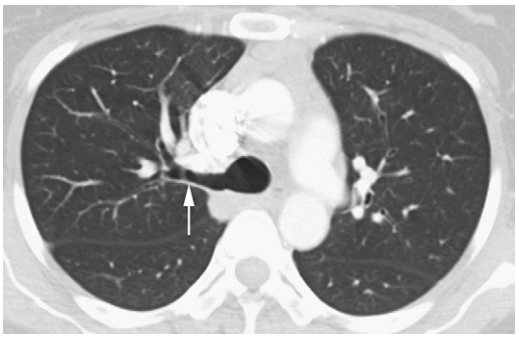

Fig. 14. Tracheal "pig bronchus." Axial CT image shows anomalous origin of entire right upper lobe bronchus (*arrow*) from the lower trachea.

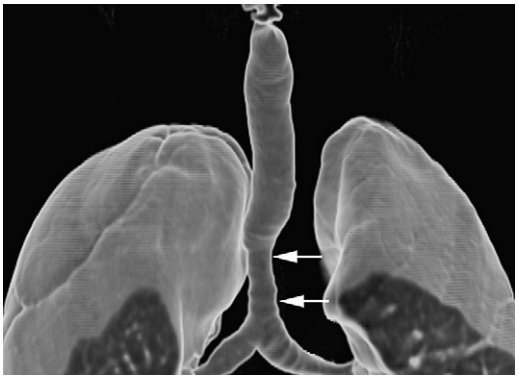

Fig. 15. Congenital tracheal stenosis. 3D external rendering of the trachea demonstrates a short-segment stenosis of the lower trachea (*arrows*).

Congenital tracheomalacia

Congenital tracheomalacia refers to softening of the trachea secondary to weakening or deficiency of cartilage, resulting in increased tracheal compliance with excessive expiratory collapse [28]. This condition is most commonly identified in premature infants, likely related to inadequate maturation of the tracheobronchial cartilage. It may also be associated with diseases involving cartilage (eg, polychondritis, chondromalacia, Hunter and Hurler syndromes) [28]. Symptoms include expiratory stridor and a barking cough.

Intervention is unnecessary in most cases because tracheal cartilage strengthens and stiffens as the child grows. Patients who do not spontaneously improve may respond to continuous positive airway pressure (CPAP) or surgical intervention (eg, aortopexy or tracheoplasty).

Congenital tracheomegaly

Congenital tracheomegaly (also referred to as Mounier-Kuhn syndrome) is characterized by dilation of the trachea and main bronchi caused by severe atrophy of longitudinal elastic fibers and thinning of the muscularis mucosa [9,64]. Affected patients typically present during the third and fourth decades with recurrent respiratory

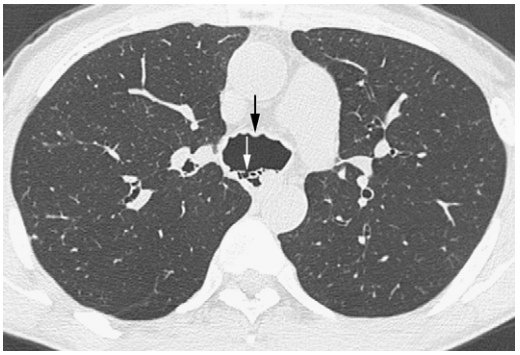

Fig. 16. Congenital tracheobronchomegaly. Axial CT image at carina level shows enlargement of tracheal lumen with corrugated configuration of anterior wall (*black arrow*) and small diverticuli posteriorly (*white arrow*).

infections. Tracheomegaly is defined in women as tracheal diameter greater than 21 mm in the coronal dimension and 23 mm in the sagittal dimension, and in men as tracheal diameter greater than 25 mm in the coronal dimension and 27 mm in the sagittal dimension [9].

On imaging studies, there is dilation of the tracheobronchial lumen, often associated with a corrugated appearance of the tracheal wall and frequent diverticula (Fig. 16). Bronchiectasis and tracheobronchomalacia are also frequently present.

Congenital tracheal diverticula

Congenital tracheal diverticula are less common than the acquired form [65]. They are characterized by single or multiple invaginations of the tracheal wall. They commonly arise 4 to 5 cm below the vocal cords or 2 to 3 cm above the carina on the right lateral aspect of the trachea. In the absence of symptoms, no treatment is necessary.

References

[1] Holbert JM, Strollo DC. Imaging of the normal trachea. J Thorac Imaging 1995;10:171–9.

[2] Naidich DP, Webb WR, Grenier PA, et al. Introduction to imaging methodology and airway anatomy. In: Naidich DP, Webb WR, Grenier PA, editors. Imaging of the airways: functional and radiologic correlations. Philadelphia: Lippincott, Williams and Wilkins; 2005. p. 1–28.

[3] Fraser RS, Colman N, Muller NL, et al. The airways and pulmonary ventilation. In: Fraser RS, Colman N, Muller NL, editors. Fraser and Pare's diagnosis of diseases of the chest. 4th edition. Philadelphia: W.B. Saunders; 1999. p. 3–70.

[4] Stern EJ, Graham CM, Webb WR, et al. Normal trachea during forced expiration: dynamic CT measurements. Radiology 1993;187(1):27–31.

[5] Naidich DP, Webb WR, Grenier PA, et al. Functional imaging of the airway. In: Naidich DP, Webb WR, Grenier PA, editors. Imaging of the airways: functional and radiologic correlations. Philadelphia: Lippincott, Williams and Wilkins; 2005. p. 181–2.

[6] Gamsu G, Webb WR. Computed tomography of the trachea: normal and abnormal. AJR Am J Roentgenol 1982;139:321–6.

[7] Vock P, Spiegel T, Fram EK, et al. CT assessment of the adult intrathoracic cross section of the trachea. J Comput Assist Tomogr 1984;8:1076–82.

[8] Breatnach E, Abbott GC, Fraser RG. Dimensions of the normal human trachea. AJR Am J Roentgenol 1983;141:903–6.

[9] Woodring JH, Smith Howard R, Rehn SR. Congenital tracheobronchomegaly (Mounier-Kuhn) syndrome: a report of 10 cases and review of the literature. J Thorac Imaging 1991;6:1–10.

[10] Greene R, Lechner GL. "Saber-sheath" trachea: a clinical and functional study of marked coronal narrowing of the intrathoracic trachea. Radiology 1975;115:265–8.

[11] Trigaux JP, Hermes G, Dubois P, et al. CT of saber-sheath trachea: correlation with clinical, chest radiographic and functional findings. Acta radiol 1994;35:247–50.

[12] Lomasney L, Bergin CJ, Lomasney J, et al. CT appearance of lunate trachea. J Comput Assist Tomogr 1989;13:520–2.

[13] Webb EM, Elicker BM, Webb WR. Using CT to diagnose nonneoplastic tracheal abnormalities. Appearance of the tracheal wall. AJR Am J Roentgenol 2000;174:1315–21.

[14] Boiselle PM, Reynolds KF, Ernst A. Multiplanar and three-dimensional imaging of the central airways with multidetector CT. AJR Am J Roentgenol 2002;179:301–8.

[15] Boiselle PM, Lee KS, Ernst A. Multidetector CT of the central airways. J Thorac Imaging 2005;20:186–95.

[16] Salvolini L, Secchi EB, Costarelli L, et al. Clinical applications of 2D and 3D CT imaging of the airways—a review. Eur J Radiol 2000;34:9–25.

[17] Naidich DP, Gruden JF, McGuiness GM, et al. Volumetric (helical/spiral) CT (VCT) of the airways. J Thorac Imaging 1997;12:11–28.

[18] Remy-Jardin M, Remy J, Artaud D, et al. Tracheobronchial tree: assessment with volume rendering—technical aspects. Radiology 1998;208:393–8.

[19] Remy-Jardin M, Remy J, Artaud D, et al. Volume rendering of the tracheobronchial tree: clinical evaluation of bronchographic images. Radiology 1998;208:761–70.

[20] Remy-Jardin M, Remy J, Deschildre F, et al. Obstructive lesions of the central airways: evaluation by using spiral CT with multiplanar and three-dimensional reformations. Eur Radiol 1996;6:807–16.
[21] Rubin GD. Data explosion: the challenge of multidetector-row CT. Eur J Radiol 2000;36:74–80.
[22] Lucidarme O, Grenier PA, Coche E, et al. Bronchiectasis: comparative assessment with thin-section CT and helical CT. Radiology 1996;200:673–9.
[23] Baroni R, Feller-Kopman D, Nishino M, et al. Tracheobronchomalacia: comparison between end-expiratory and dynamic-expiratory CT methods for evaluation of central airway collapse. Radiology 2005;2:635–41.
[24] Nishino M, Hatabu H. Volumetric expiratory HRCT imaging with MSCT. J Thorac Imaging 2005;20:176–85.
[25] Choi SJ, Choi BK, Kim HJ, et al. Lateral decubitus HRCT: a simple technique to replace expiratory CT in children with air trapping. Pediatr Radiol 2002; 32:179–82.
[26] Long FR, Williams RS, Adler BH, et al. Comparison of quiet breathing and controlled ventilation in the high-resolution CT assessment of airway disease in infants with cystic fibrosis. Pediatr Radiol 2005; 35:1075–80.
[27] Goo HW, Kim HJ. Detection of air trapping on inspiratory and expiratory phase images obtained by 0.3-second cine CT in the lungs of free-breathing young children. AJR Am J Roentgenol 2006;187: 1019–23.
[28] Carden K, Boiselle PM, Waltz D, et al. Tracheomalacia and tracheobronchomalacia in children and adults: an in-depth review of a common disorder. Chest 2005;127:984–1005.
[29] Boiselle PM, Feller-Kopman D, Ashiku S, et al. Tracheobronchomalacia: evolving role of mutlislice helical CT. Radiol Clin North Am 2003;41:627–36.
[30] Fraser RS, Colman N, Müller NL, et al. Upper airway obstruction. In: Fraser RS, Colman N, Müller NL, editors. Fraser and Pare's diagnosis of diseases of the chest. 4th edition. Philadelphia: W. B. Saunders Co; 1999. p. 2033–6.
[31] Prince JS, Duhamel DR, Levin DL, et al. Nonneoplastic lesions of the tracheobronchial wall: radiographic findings with bronchoscopic correlation. Radiographics 2002;22:S215–30.
[32] Sun M, Ernst A, Boiselle PM. MDCT of the central airways: comparison with bronchoscopy in the evaluation of complications of endotracheal and tracheostomy tubes. J Thorac Imaging 2007;22:136–42.
[33] Houston HE, Payne WS, Harrison EG Jr, et al. Primary cancers of the trachea. Arch Surg 1969;99: 132–40.
[34] Dennie CJ, Coblentz CL. The trachea: pathologic conditions and trauma. Can Assoc Radiol J 1993; 44:157–67.
[35] McCarthy MJ, Rosado-de-Christenson ML. Tumors of the trachea. J Thorac Imaging 1995;10:180–98.
[36] Grillo HC, Mathisen DJ. Primary tracheal tumors: treatment and results. Ann Thorac Surg 1990;49: 69–77.
[37] Okike N, Bernatz PE, Woolner LB. Carcinoid tumors of the lung. Ann Thorac Surg 1976;22:270–7.
[38] Parsons RB, Milestone BN, Adler LP. Radiographic assessment of airway tumors. Chest Surg Clin N Am 2003;13:63–77.
[39] Kaminski JM, Langer CJ, Movsas B. The role of radiation therapy and chemotherapy in the management of airway tumors other than small-cell carcinoma and non-small-cell carcinoma. Chest Surg Clin N Am 2003;13:149–67.
[40] Kwong JS, Adler BD, Padley SPG, et al. Diagnosis of diseases of the trachea and main bronchi: chest radiography vs CT. AJR Am J Roentgenol 1993;161: 519–22.
[41] Kwak SH, Lee KS, Chung MJ, et al. Adenoid cystic carcinoma of the airways: helical CT and histopathologic correlation. AJR Am J Roentgenol 2004;183: 277–81.
[42] Johnson TH, Mikita JJ, Wilson RJ, et al. Acquired tracheomalacia. Radiology 1973;109:576–80.
[43] Jokinen K, Palva T, Sutinen S, et al. Acquired tracheobronchomalacia. Ann Clin Res 1977;9:52–7.
[44] Palombini BC, Villanova CA, Araujo E, et al. A pathogenic triad in chronic cough: asthma, postnasal drip syndrome and gastroesophageal reflux disease. Chest 1999;116:279–84.
[45] Ikeda S, Hanawa T, Konishi T, et al. Diagnosis, incidence, clinicopathology and surgical treatment of acquired tracheobronchomalacia. Nihon Kyobu Shikkan Gakkai Zasshi 1992;30:1028–103 [in Japanese].
[46] Hasegawa I, Boiselle PM, Hatabu H. Bronchial artery visualization on multislice CT in patients with acute PE: comparison with chronic or recurrent PE. AJR Am J Roentgenol 2004;182:67–72.
[47] Lee KS, Ernst A, Trentham D, et al. Prevalence of functional airway abnormalities in relapsing polychondritis. Radiology 2006;240:565–73.
[48] Gilkeson RC, Ciancibello LM, Hejal RB, et al. Tracheobronchomalacia: dynamic airway evaluation with multidetector CT. AJR Am J Roentgenol 2001;176:205–10.
[49] Zhang J, Hasegawa I, Feller-Kopman D, et al. Dynamic expiratory volumetric CT imaging of the central airways: comparison of standard-dose and low-dose techniques. Acad Radiol 2003;10:719–24.
[50] Lee KS, Sun ME, Ernst A, et al. Comparison of dynamic expiratory CT with bronchoscopy in diagnosing airway malacia. Chest 2007;131: 758–64.
[51] Wilson TA, Rodarte JR, Butler JP. Wave speed and viscous flow limitation. In: Macklem PT, Mead J, editors. Handbook of physiology, the respiratory system. Mechanics of breathing, part 1, vol. 3. Bethesda (MD): The American Physiological Society; 1986. p. 55–61.

[52] Heussel CP, Hafner B, Lill J, et al. Paired inspiratory/expiratory spiral CT and continuous respiration cine CT in the diagnosis of tracheal instability. Eur Radiol 2001;11:982–9.
[53] Aquino SL, Shepard JA, Ginns LC, et al. Acquired tracheomalacia: detection by expiratory CT scan. J Comput Assist Tomogr 2001;25(3):394–9.
[54] Boiselle PM, Ernst A. Tracheal morphology in patients with tracheomalacia: prevalence of inspiratory "lunate" and expiratory "frown" shapes. J Thorac Imaging 2006;21:190–6.
[55] Murgu SD, Colt HG. Recognizing tracheobronchomalacia. J Respir Dis 2006;27:327–35.
[56] Baroni RH, Ashiku S, Boiselle PM. Dynamic-CT evaluation of the central airways in patients undergoing tracheoplasty for tracheobronchomalacia. AJR Am J Roentgenol 2005;184:1444–9.
[57] Ghaye B, Szapiro D, Fanchamps JM, et al. Congenital bronchial abnormalities revisited. Radiographics 2001;21:105–19.
[58] Zylak CJ, Eyler WR, Spizarny DL, et al. Developmental lung anomalies in the adult: radiologic-pathologic correlation. Radiographics 2002;22:S25–43.
[59] McGuinness G, Naidich DP, Garay SM, et al. Accessory cardiac bronchus: computed tomographic features and clinical significance. Radiology 1993; 189:563–6.
[60] Ali MI, Brunson CD, Mayhew JF. Failed intubation secondary to complete tracheal rings: a case report and literature review. Paediatr Anaesth 2005;15: 890–2.
[61] Faust RA, Stroh B, Rimell F. The near complete tracheal ring deformity. Int J Pediatr Otorhinolaryngol 1998;45:171–6.
[62] Boiselle PM, Ernst A, DeCamp M. CT diagnosis of complete tracheal rings in an adult patient. J Thorac Imaging 2007;22:169–71.
[63] Rutter MJ, Willging JP, Cotton RT. Nonoperative management of complete tracheal rings. Arch Otolaryngol Head Neck Surg 2004;130:450–2.
[64] Shin MS, Jackson RM, Ho K. Tracheobronchomegaly (Mounier-Kuhn syndrome): CT diagnosis. AJR Am J Roentgenol 1988;150:777–8.
[65] Soto-Hurtado EJ, Penuela-Ruiz L, Rivera-Sanchez I, et al. Tracheal diverticulum: a review of the literature. Lung 2006;184:303–7.